Geothermal flow and water-load seafloor depth of the Eastern Mediterranean Sea

Cite as: AIP Conference Proceedings **2123**, 020018 (2019); https://doi.org/10.1063/1.5116945
Published Online: 17 July 2019

Elie El Jbeily, Massimo Verdoya, Paolo Chiozzi, Roberta Ivaldi, and Afif Ghaith

Geothermal Flow and Water-Load Seafloor Depth of the Eastern Mediterranean Sea

Elie El Jbeily[1,a)], Massimo Verdoya[1], Paolo Chiozzi[1], Roberta Ivaldi[1,2], Afif Ghaith[3]

1DISTAV, Università di Genova, Italy
2 Istituto Idrografico Marina
3Università di Ferrara, Italy
a) elie_lebnavy@hotmail.co.uk

Abstract. We used bathymetry, sediment thickness and terrestrial heat-flow data to investigate the nature of the Eastern Mediterranean Sea lithosphere. We processed bathymetric data by removing the subsidence caused by sediment deposition to obtain the water-loaded seafloor depth. Terrestrial heat flow measurements were corrected for sedimentation and climatic changes to infer the purely conductive steady-state geothermal flow. Water-load seafloor depths and thermal data were then compared to reference models of continental lithosphere stretching and ocean plate cooling. The results argue that the Levantine Basin is floored by a continental stretched crust that thinned by a factor of 1.6-2.7, whereas the Herodotus Basin crust is of oceanic type. The water-loaded seafloor depths in all the Eastern Mediterranean are consistent with geological ages of > 250 Ma. The mantle heat flow in the Herodotus Basin (33 mW m^{-2}) is consistent with that of the oceanic Ionian lithosphere, whereas in the Levantine Basin (26 mW m^{-2}) is comparable to that of the Sinai continental microplate.

INTRODUCTION

The Eastern Mediterranean Sea is a geologically complex region with remarkable structural features that have formed through a long tectonic history since, at least, the Permian. From the bathymetry, different morphological features can be distinguished, namely the Cyprus Arc, the Mediterranean and Latakia ridges, the Eratosthenes Continental Block, the Nile delta cone, the Herodotus and the Levantine basins and the Florence Rise (Fig. 1).

The nature and age of the crust of this realm is still widely debated. It has been suggested to preserve parts of the southern Neo-Tethys ocean, which formed by the middle Permian, or even of the early Devonian Paleo-Tethys ocean (e.g. Garfunkel, 1998; Stampfli et al., 1991; Domeier and Torsvik, 2004; Inati et al., 2016). So far, the location of the remnants of these ancient oceans and their age have never been clearly identified, likely due to the exceptionally thick sedimentary cover (often exceeding 10 km), overlying the crystalline crust, that limit the efficiency of geophysical approaches. As a result, the pattern of the ancient seafloor spreading systems is rather uncertain.

The nature of the crust underlying the Levantine Basin is still a matter of debate. It has been suggested that the easternmost sector, whose early evolution is closely related to the history of the Neo-Tethys, is underlain by stretched continental crust, which underwent rifting in the Late Paleozoic-Early Mesozoic (Netzeband et al., 2006; Gardosh et al., 2006). Other authors instead argue for an old oceanic crust, with the age varying from Triassic to Cretaceous (e.g. Dercourt et al., 1986), or a mixture of continental and oceanic crust, depending on the different tectonic evolutions of rifting and subduction (Robertson, 1998; Ben-Avraham et al., 2002). West of the Levantine Basin, a very thin crystalline crust, likely oceanic, occurs in the Herodotus Basin, with a thickness between 6 and 10 km (Inati et al., 2016).

The analysis of the sediment load-corrected basement depth, also referred to as water-loaded depth of seafloor (*WLD*), as a function of crustal age, coupled with terrestrial heat flow observations, has been suggested as a powerful tool to discriminate the nature of the crust and to highlight the occurrence of mantle dynamic processes. This approach has been extensively used in oceanic realms on a global scale (e.g. Crosby and McKenzie, 2006; Hoggard et al., 2017; Chiozzi and Verdoya, 2018 and references therein) and continental regions (e.g. Pasquale et al. 1994) that underwent extensional processes and basin formation, such as the western Mediterranean. *WLD* provides quantitative information that helps understand not only the tectonics, but also the crustal structure and density variations at depth. In ocean lithosphere, topography and heat flow depend on geological age, for *WLD* is controlled by thermal isostasy, i.e. the increase of subsidence with time caused only by cooling of the ocean plate. In continental rifting realms, lithosphere thinning is accompanied by initial warming followed by temperature decrease and subsequent increase of *WLD* (subsidence) with time (McKenzie, 1978; Pasquale et al., 1995).

Technologies and Materials for Renewable Energy, Environment and Sustainability
AIP Conf. Proc. 2123, 020018-1–020018-12; https://doi.org/10.1063/1.5116945
Published by AIP Publishing. 978-0-7354-1863-9/$30.00

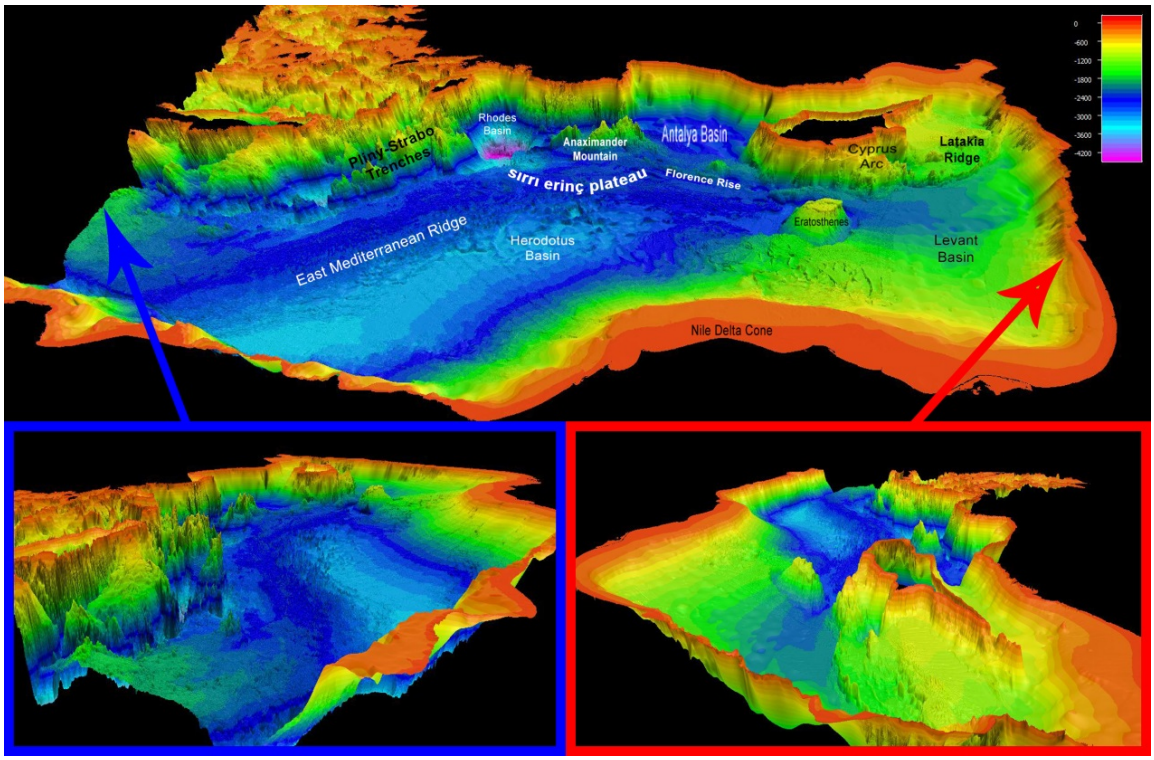

FIGURE 1. Exaggerated 3D views of the Eastern Mediterranean seafloor; insets: view from West (left) and East (right). The main morphological and tectonic seabed features and basins are shown. Bathymetry scale is in meters.

In this paper, we use data of sediment load-corrected basement depth for investigating the nature of the Eastern Mediterranean lithosphere and review the available geothermal flow data to constrain the nature of the lithosphere. Heat-flow information also supplies a first insight into the lithosphere thermal state and thus forms a basis for future studies on the potential for renewable energy in the region. We start our analysis by processing bathymetry and heat-flow data obtained from direct measurements and removing effects of sediment deposition, and paleoclimatic changes. We calculate the seafloor *WLD* and the corrected heat flow, which are then compared to predictions obtained by applying reference models of ocean lithosphere cooling and continental stretching. The results allow discriminating between oceanic and continental realms of the Eastern Mediterranean lithosphere.

DATABASES

Bathymetry

Even if ocean and sea bathymetry is far from being completely surveyed, global bathymetric datasets are available through the collection of a number of surveys. Among the several sources, all with different resolutions and uncertainty, we adopted for this study those from the European Marine Observation and Data Network (EMODnet). This database is a 0.125x0.125 arc minutes (about 330x330 meters) digital terrain model resulting from collecting high-resolution single and multibeam echo sounders bathymetric surveys, composite DTMs and satellite-derived bathymetry data (http://www.emodnet.eu/data). Gaps in the database were filled with the General Bathymetric Chart of the Oceans (GEBCO; https://www.gebco.net/).

It must be stressed that satellite derived bathymetry can be biased and can lack of precision. On the other hand, ship sounding coordinates using old positioning systems are subject to meters of horizontal error. New high-resolution and accurately positioned bathymetric data are not available everywhere and limited to coastal areas or along ship tracks.

A bathymetric map of the Eastern Mediterranean is presented in Figure 1. The northeastern sector includes the Rhodes, Finike and Antalya basins to the north and the Anaximander Ridge to the south. This sector is the junction between the northwest-southeast trending Florence Rise and the northeast-southwest trending Pliny-Strabo trenches. In this sector, bathymetry reaches a maximum value of 4600 m in the Rhodes Basin, a deep trough between Rhodes island to the east and southwestern Turkey to the west, where the Finike Basin deepens to 3000 m. Aksu et al. (2017), describe the Anaximander Mountains as three prominent bathymetric highs: the Anaximander Mountain, i.e an open V-shaped narrow and arcuate ridge with its crest at 1100 m depth; the Anaximenes Mountain, a northeast-southwest trending broadly arcuate ridge with its crest at 750 m depth; the Anaxagoras Mountain, a northwest-southeast trending broad bathymetric high with several prominent peaks at 950-1200 m water depth. The Sirri Erinç Plateau is a prominent arcuate zone characterized by corrugated seafloor located between the Anaximander Mountain and the combined

Anaximenes and Anaxagoras Mountains, with depths ranging from 2100 m in the northeast (Finike Basin) to 3500 m in the west (Rhodes Basin) and in the southwest.

The Antalya Basin is situated in a forearc setting between the Florence Rise and the Cyprus Arc, southwest of Turkey whereas the Adana Basin occurs southeast of Turkey (Işler et al. 2005).The Hecataeus Seamount or Rise to the south of Cyprus is characterized by a shallow seabed reaching minimum depths of 230 m below sea level. Hecataeus Rise has a southeast extension from the southern coast of Cyprus and then gradually merges with the Latakia Ridge. It constitutes the southern deformation front of the Cyprus Arc separating the Levantine Basin in the south from the Cyprus Basin in the north. In the east, the expression of the ridge changes to a number of narrow, northeast-trending ridges and basins (Hall et al. 2005; Welford et al., 2015).

The Latakia Ridge separates the Latakia Basin from the Levantine Basin, which has a bathymetry reaching 2000 m in the central part ("abyssal plain") and a maximum value of 2600 m west of the Eratosthenes Seamount, which constitutes its western boundary. It has a narrow shelf to the East (Lebanon – Northern Israel coast) that gets slightly larger to south-east (Southern Israel – Sinai). The southern limit of the basin shows instead a relatively wider shelf (sediment disposal from the Nile delta). In general, the Levantine Basin is characterized by a steep slope where water can suddenly increase from 100-200 m to 1000-1500 m. In front of Lebanon, the slope toe is cut by fault scarps, deeply indented by sea valleys, a submarine promontory and submarine flat-floored canyons (Inati et al. 2016).

South of Cyprus and west of the Levantine Basin, the Eratosthenes seamount forms a remarkably elevated seabed feature, with 1900 m height from the surrounding seafloor, and a depth of 700 m. Southwest of the Levantine Basin, the Nile delta Basin extends, with its submerged sediment fan characterized by depths ranging between 400 and 1600 m. It is followed to the West by the Herodotus Basin with depths reaching 3200 m in the center of the basin. In the Herodotus Basin, the Mediterranean Ridge extends from Calabria to Turkey, passing south of Crete (Hellenic Arc) and continuing eastwards, south of Cyprus.

Terrestrial Heat Flow

Surface heat-flow determinations, collected during several surveys since the 1970s, are available for the investigated area. Marine data (twenty-one values) were mostly obtained with the classical Ewing probe penetrating the seafloor sediments (Erickson, 1970; Erickson et al., 1977) and six values were inferred from temperature logging in deep-sea boreholes (Erickson and Von Herzen, 1978; Pribnow et al., 2000). Thirty-three data were also available on Cyprus island measurements in shallow boreholes for water and mineral exploration (Morgan, 1973 and 1979). Data are contained in the database of the International Heat Flow Commission (IHFC; http://www.heatflow.und.edu/index2.html).

The locations of marine heat flow data obtained with the Ewing probe are rather uniformly spaced throughout the eastern Mediterranean. The penetrations achieved with the probes varied between 2.5 and 11.5 meters. The observed heat-flow ranges between 11 and 44 mW m^{-2}. In our analysis, we took into account only measurement sites with penetration depth > 2.5 m and more than one measured temperature. Moreover, we rejected sites wherein failure of the probe to achieve thermal equilibrium was recorded. Our final heat-flow database consists of eighteen determinations that give an average observed heat flow of 26±8 mW m^{-2}.

In the borehole 376, located on the Florence Rise west of Cyprus, five down-hole temperature measurements were carried out in the frame of the Deep Sea Drilling Project, Leg 42A (Erickson and Von Herzen, 1978). Temperature measurements vary widely in quality. Using only bottom water temperature and the uppermost three temperature values, an average temperature gradient of 33±15 mK m^{-1} was determined in the depth range 0-74 m. By assuming a harmonic mean of the thermal conductivity values in the same depth interval, an observed heat flow of 39 ± 15 mW m^{-2} was estimated.

Pribnow et al. (2000) reanalyzed in a standard systematic manner geothermal measurements made with temperature probes, during Ocean Drilling Program (ODP) Leg 160. The combination of available thermal conductivity data from five sites, reduced to in-situ conditions, and the recorded thermal gradients yielded heat flow values, calculated with the Bullard method, ranging from 8 mW m^{-2} to 84 mW m^{-2}. We suggest that the lowest values could be affected by advective heat transfer. We thus attempted to improve the quality of the dataset by rejecting sites characterized by thermal gradient lower than 8 mK m^{-1} and with only two temperature records. After this selection, only the hole 967A and 968A, located between Cyprus and Eratosthenes Seamount show high quality thermal data and observed heat flow ranges from 57 to 84 mW m^{-2}.

In Cyprus, temperatures were recorded in boreholes ranging in depth from 85 to 399 m and produced heat flow values varying from 6 to 46 mW m^{-2}. After a careful data inspection, we rejected heat flow values obtained from temperature logs denoting evident effects of heat transfer by water movement or lacking thermal conductivity determinations and detailed stratigraphic information. The observed heat flow values from the twelve most reliable thermal logs is fairly uniform and low, ranging from 19 to 40 mW m^{-2}, with an average value of 28±6 mW m^{-2}.

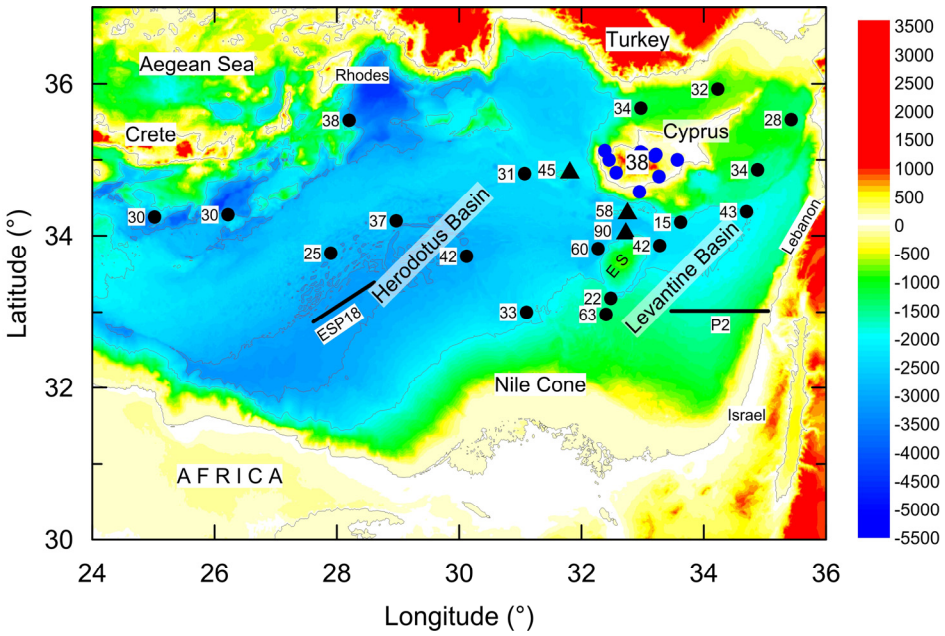

FIGURE 2. Bathymetry (in m) and heat-flow data (in mW m^{-2}) corrected for terrain effects: marine conventional (black full circle) by Erickson (1970) and Erickson et al. (1977), DSDP-ODP drilling (black full triangle) by Pribnow et al. (2000), water, mineral and oil exploration borehole (blue full circle) by Morgan (1973 and 1979). Seismic profiles: ESP18 by de Voogd et al. (1992) and P2 by Netzeband et al. (2006). ES= Eratosthenes seamount.

DATA PROCESSING

Estimation of the Seafloor Water-Loaded Depth

We estimated *WLD* as the actual bathymetry corrected for the sediment loading. The sediment correction assumes Airy isostasy and replaces sedimentary mass with equivalent mass of water and asthenospheric mantle (e.g. Sawyer, 1985). Calculation implies the knowledge of thickness of the sediment overlying the crystalline crust (basement).

Due to the regional character of our study and in the light of the uneven coverage of the available seismic profiles giving detailed information on the crustal structure and composition, data on sediment thickness for the Eastern Mediterranean were extracted from the Crust 1.0 model (https://igppweb.ucsd.edu/~gabi/crust1.html), which incorporates the global sediment thickness database by Laske et al. (2013). This database was obtained from published digital high-resolution maps and hand-digitized atlases and maps, and contains data with a 1°x1° spatial resolution. Therefore, we averaged bathymetry data and calculated the sediment correction and *WLD* over 1x1 degree bins.

The sedimentary correction assumes that basement was initially aligned with sea level before the basin formation. In our approach, it is also assumed that the crust has no flexural rigidity. Sawyer (1985) has shown that flexural loading and a local isostatic model will be similar in regions where sediment has nearly uniform lateral thickness at all nearby points (Heine et al., 2008). This condition is reasonably applicable at least in the central portions of the Eastern Mediterranean.

The sedimentary correction, c_s, is thus given by

$$c_s = \frac{\rho_a - \rho_s}{\rho_a - \rho_w} h_s \tag{1}$$

where $\rho_a = \rho_m(1 - \alpha T_a)$ is the asthenosphere density, ρ_m is lithospheric mantle density at room temperature, T_a the asthenosphere temperature, α the thermal expansion coefficient, ρ_w the seawater density, ρ_s the bulk density of the sedimentary column, and h_s is the sedimentary column thickness. The bulk density increases with sediment compaction as it depends on fluid in the pore space and the solid grains. Assuming an exponential decrease of porosity as a function of depth, the change of density within the sedimentary column is

$$\rho_s = \rho_{sg} + \frac{\phi_o \lambda}{z}(\rho_w - \rho_{sg})\left(1 - e^{\frac{-z}{\lambda}}\right) \tag{2}$$

where ρ_{sg} is the solid grain density, ϕ_o the porosity of sediment at depth z=0, and λ the compaction decay length scale for oceanic sediments. Parameters adopted for calculations are listed and referenced in Table 1. By studying borehole data from the Southern Tyrrhenian, Pasquale et al. (2007) suggested ρ_{sg} = 2740 kg m^{-3}, ϕ_o = 0.71 and λ = 640 m. Since sediment types and depositional sequences are very similar in the central-eastern Mediterranean, these values can be adopted also for the Eastern Mediterranean.

TABLE 1. List of parameters used in calculations

Symbol	Value	Reference
ρ_w	1030 kg m^{-3}	-
ρ_m	3300 kg m^{-3}	Hoggard et al. (2017)
ρ_{co}	2780 kg m^{-3}	Le Pichon and Sibuet (1981)
α	3 10^{-5} °C^{-1}	Hoggard et al. (2017)
T_a	1330 °C	Hoggard et al. (2017)
h	30 km	Netzeband et al. (2006)
H	125 km	Schütz et al. (2014)

Figure 3 shows the expected change of the bulk density of sediments together with sediment correction as a function of depth, whereas the calculated *WLD* is presented in Fig. 4. The sediment correction increase rapidly if the sedimentary column is thinner than 2000 m, then it has a linear trend with a rate of 250 m per kilometer of sediment.

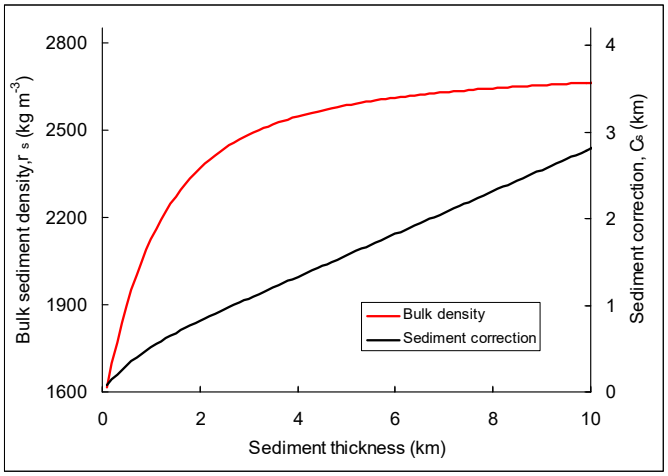

FIGURE 3. Bulk sediment density (ρ_s) and sediment correction (c_s) plotted as a function of sediment thickness.

For an average sediment thickness in the Eastern Mediterranean of about 8 km, the correction is 2300 m. *WLD* exhibits maximum values (5.6-6.0 km) in the deepest portion of the investigated area (average bathymetry ~ 3000 m), i.e. the abyssal plain of the Herodotus and Rhodes basins. Although the bathymetry is shallower (~ 1300 m) in the Levantine Basin, *WLD* is significantly large as well (4.5 km), for the sedimentary layer overlying the crystalline crust is as thick as ~ 8 km.

Corrected Heat Flow

Figure 2 shows the selected heat flow values after correction for terrain effects. Several effects, such as thermal refraction, sedimentation, climatic changes, topography and uplift/erosion, are in principle capable of causing heat flow to be bias the true, purely conductive steady-state heat flow. Thermal refraction, i.e. preferential flow of heat through high-thermal conductivity structures, such as salt domes, may be one cause of strong local variability in the heat-flow measurements. This disturbance does not appear to be relevant, as salt layer (Messinian evaporites) seems rather uniform in thickness and ubiquitous in the investigated area (Erickson and Von Herzen, 1978).

Sedimentation and long-term changes in the sea-floor temperature can instead be major effects that bias the observed heat flow. Erickson et al. (1977) attempted a correction for sedimentation, however the poor knowledge of sedimentation rate yielded only rough estimates. In the light of the stratigraphic and climatic data achieved to date, we reprocessed the observed heat flow dataset to remove such thermal effects.

We evaluated the blanketing effect only due to the most recent sedimentation (Plio-Quaternary) by means of the simplified approach by Von Herzen and Uyeda (1963), which is based on the assumption of a constant sedimentation rate with a thermal diffusivity of 9.5 m^2 a^{-1} and no compaction or associated fluid expulsion (Chiozzi and Verdoya,

2018). The Plio-Quaternary deposition cycle was assumed as a single event, which took place on the Miocene formations acting as a basement. Values of sediment thickness were extracted from the seismic isochron map of Genesseaux et al. (1998) by assuming a uniform velocity of 2000 m s^{-1} in the Plio-Quaternary layer.

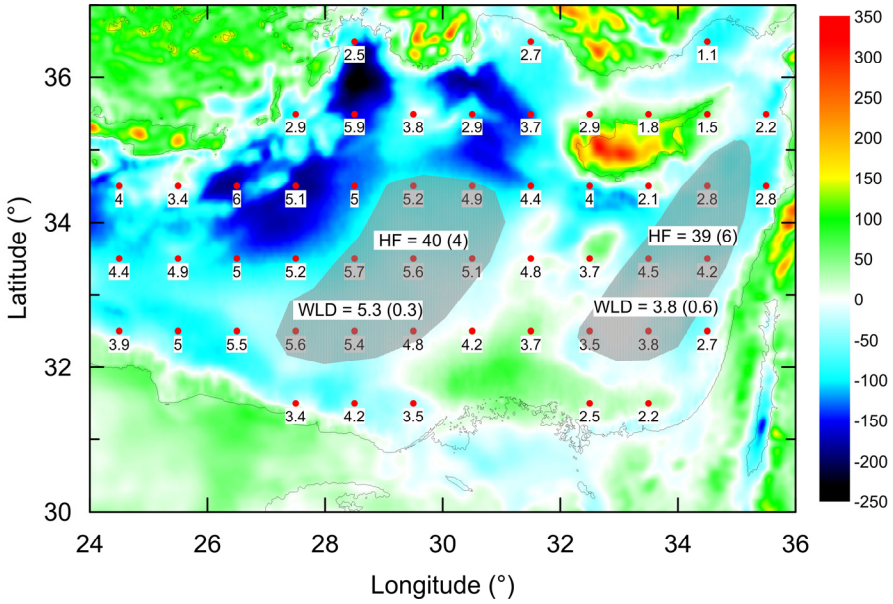

FIGURE 4. Location of the water-loaded depth (*WLD*) sites (full red circle, value in km) superimposed on a free-air gravity anomaly (Sandwell et al., 2014), c*olour contour* interval in mGal. The grey areas are those selected for *WLD* analyses since likely unaffected by thickened crust, flexural moats and subduction (see text for details). In these areas, average values of *WLD* and terrestrial heat flow (HF) are indicated. Standard deviation is in brackets.

The correction for the temperature variation in response to paleoclimatic changes was also evaluated for both marine and on land data. The marine data correction was based on the paleoclimate model proposed by Pasquale et al. (2005) for the central Mediterranean, which allows for the climatic history of the Mediterranean Sea. Generally, the temperature history of the bottom water in the central-eastern Mediterranean shows smaller changes than in the western part of the basin. With respect to the last 8 ka, during which no change has occurred, we assumed a decrease of 3 °C from 700 to 135 ka ago, i.e., half of that of the western Mediterranean. Cooling was followed by three other cold periods. The lowest temperature occurred in the period between 82 and 18 ka ago. By considering average thermal diffusivity and conductivity values of Plio-Quaternary sediment, the climatic correction near the surface is, in terms of heat flow, about 4 mW m^{-2}.

Morgan (1979) suggested that the climatic correction would increase the heat-flow values of Cyprus database on an average by 4.0 mW m^{-2}. We revised this correction by taking into account the new climatic model for southern Europe proposed by Majorowicz and Wybraniec (2011). The palaeoclimatic correction as a response to five glacial cycles since 600 kyr ago with glacial–interglacial surface temperature amplitude of 7 °C was calculated for a homogeneous thermal conductivity (2 W m^{-1} K^{-1}), diffusivity (28.4 m^2 a^{-1}) and basal heat flow (60 mW m^{-2}). Such past temperature changes caused a heat flow reduction, which smoothes with depth. The correction is about 10 mW m^{-2} in the depth range of temperature measured in the Cyprus boreholes. Topography effect is generally less than 10% and uplift and erosion were difficult to apply, due to uncertainties in the parameters required for these corrections (Morgan, 1979).

CRUST NATURE

The analysis of the water-load depth of seafloor (*WLD*) permits to evaluate the nature of the lithosphere on the basis of the expected subsidence for an uniform extension model together with a cooling model of an ocean plate (e.g. McKenzie, 1978; Le Pichon and Sibuet, 1981; Sawyer, 1985; Pasquale et al., 1994; Chiozzi and Verdoya, 2018). Besides continental stretching and ocean lithosphere cooling, other younger and still active geodynamic processes, such as subduction and crustal thickening, are affecting the investigated area. These processes are likely to produce seamounts (thickened crust) and flexural moats that may bias the estimation of *WLD*.

To exclude from the analysis those parts of the Eastern Mediterranean Sea wherein *WLD* is not simply controlled by thermal isostasy associated to ocean plate cooling and/or continental lithosphere thinning, we followed the criterion relying on the analysis of free-air gravity anomaly data (see Crosby et al., 2006; Crosby and McKenzie, 2009). Figure 4 presents a map of the free air gravity anomaly in the Eastern Mediterranean Sea. We notice that seamounts (such as Heratosthenes) and bathymetric highs (Nile Cone) are rather clearly visible in the bathymetric map, whereas moats

(southeast of Rhodes and Crete, south of Cyprus) are little perceivable, for they are filled with sediment (Fig. 2). However, they are associated with clear negative gravity anomalies. Therefore, we excluded from our analyses sectors of gravity minima and maxima corresponding to moats and seamounts, respectively. In those parts of the Herodotus and Levantine basins with negligible free-air gravity anomaly (Fig. 4), which are more likely to reflect processes related to lithosphere stretching and plate cooling, the average *WLD* is 5.3 and 3.8 km, respectively.

As a first step, we checked whether such *WLD* values fit a continental lithosphere pure-shear stretching model (McKenzie, 1978). The model envisions a first stage, represented by thinning of the crust and lithospheric mantle, and by asthenosphere upwarping. Contemporaneously, initial subsidence by isostatic rebound takes place, because of the density change resulting from stretching and temperature increase of the uppermost mantle. Subsequently, a passive process caused by the lithosphere comeback to thermal equilibrium, with consequent lithosphere contraction, results in a long-term thermal subsidence. Stretching is assumed instantaneous and uniform, and the lithosphere thickness H is reduced by a factor β.

If the compressibility effect on the crust, ρ_c, and lithospheric mantle, ρ_H, density is neglected, the initial subsidence WLD_i is given by (Le Pichon and Sibuet, 1981; Pasquale et al., 1994):

$$WLD_i = \frac{H\rho_a - h\rho_c - (H-h)\rho_H}{\rho_a - \rho_w}\left(1 - \frac{1}{\beta}\right) \tag{3}$$

with H the lithosphere thickness, $\rho_c = \rho_{co}\left(1 - \frac{\alpha}{2}T_a\frac{h}{H}\right)$ and $\rho_H = \rho_m\left(1 - \frac{\alpha}{2}T_a - \frac{\alpha}{2}T_a\frac{h}{H}\right)$, where ρ_{co} is crust density at room temperature and h the crust thickness.

At infinite time, the lithosphere attains thermal equilibrium with a maximum *WLD* expressed by

$$WLD_\infty = h\frac{\rho_H - \rho_c + \rho_m(\alpha/2)T_a + \varepsilon}{\rho_a - \rho_w}\left(1 - \frac{1}{\beta}\right) \tag{4}$$

where $\varepsilon = -\frac{\rho_m - \rho_{co}}{\beta}\left(\frac{\alpha h}{2H}T_a\right)$ can be neglected since it yields an error on the order of 0.5%.

The assumed values for h, H, ρ_{co}, ρ_m, ρ_w, α and T_a are listed in Table 1. It follows that eq (3) becomes:

$$WLD_i = 3.4\left(1 - \frac{1}{\beta}\right) \qquad \text{[km]} \tag{5}$$

and eq (4)

$$WLD_\infty = 7.3\left(1 - \frac{1}{\beta}\right) \qquad \text{[km]} \tag{6}$$

As the thermal subsidence follows approximately an exponential law with time constant $\tau = H^2\pi^{-2}\chi^{-1}$, for a continental lithosphere with thermal diffusivity χ= 32 m^2 a^{-1}, the water-load depth as a function of time and stretching factor, WLD_c, is obtained by combining eq (5) and (6)

$$WLD_c = \left[3.4 + 3.9\left(1 - e^{\frac{t}{\tau}}\right)\right]\left(1 - \frac{1}{\beta}\right) \qquad \text{[km]} \tag{7}$$

Curves of *WLD* as a function of β calculated at different times since rifting by means of eq (7) are shown in Fig. 5, together with the *WLD* values inferred over a 1x1 degree bins and located in the null free-air anomaly sectors of the Levantine and Herodotus basins (Fig. 4). After ~ 200 Ma, the stretched lithosphere is nearly in thermal equilibrium and thus *WLD* no longer increases with time. *WLD* data from the Levantine Basin plot on the t >150-250 Ma curves and stretching factor spanning from 1.6 and 2.7. *WLD*s of the Herodotus Basin span within a relatively smaller range and significantly exceed (> 1 km) those predicted by the continental stretching model.

Pasquale et al. (1994) interpreted the *WLD*s excess in the northwestern Mediterranean continental stretched crust as due to effect of the present-day compressive tectonic regime. In the Herodotus Basin, the nearly negligible seismic activity (Salamon et al., 1996) seems indicating that the lithosphere instead behaves as a passive block. Thus, the *WLD* excess would not be related to the present-day stress regime.

It has been suggested that when β is greater than 3.2, the asthenospheric material should be able to rise for lithostatic pressure and to break through a thinned continental crust to form new crust of oceanic type (Le Pichon and Sibuet., 1981; Sawyer, 1985; Pasquale et al., 1994). At some *WLD* sites of the Herodotus Basin factor β exceeds 3.2 (Fig. 5). Moreover, the terrestrial heat flow within the sector of null gravity anomaly ranges between 37 and 42 mW m^{-2}. In the central Mediterranen (Ionian Sea) Pasquale et al. (2005) found that the oceanic realm seems characterized by a terrestrial heat-flow of about 40 mW m^{-2}. Thus, the *WLD* and stretching excess as well as the surface heat flow argue for the oceanic nature of the Herodotus Basin.

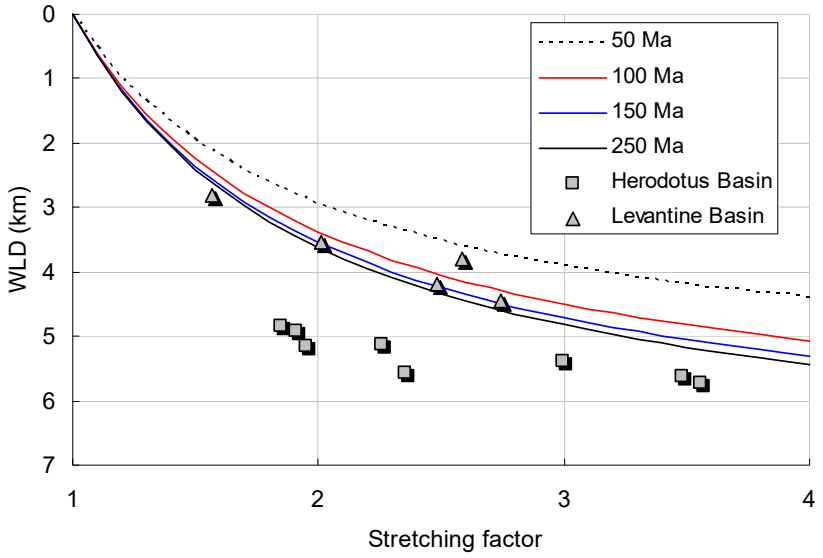

FIGURE 5. Average water-load seafloor depth (*WLD*) in the Herodotus and Levantine basins (grey areas in Fig. 4) compared to a *WLD* versus stretching factor (β) model, for a continental breakup ages of 50-250 Ma. The thermal time constant (τ) value is 62.8 Ma.

From global scale observations, several relationships between *WLD*s and oceanic crust age by means of plate or half-space cooling models were suggested (e.g. Parsons and Sclater, 1977; Stein and Stein, 1992; Crosby et al., 2006). Recent studied by Hoggard et al. (2017) confirmed that the plate model provides a better explanation for the water-load seafloor depth of oceanic lithosphere as function of time. With this model, the water-load seafloor depth of oceanic lithosphere, WLD_o, is (Turcotte and Schubert, 2002)

$$WLD_o = d + \left(\frac{\rho_m \alpha T_a H_o}{2(\rho_m - \rho_w)}\right)\left\{1 - \frac{8}{\pi^2}\sum_{n=0}^{\infty}\frac{1}{(1+2n)^2}\exp\left[\frac{-\chi(1+2n)^2\pi^2 t}{H_o^2}\right]\right\} \quad (8)$$

where d is the zero-age depth, H_o is the thickness of the oceanic lithospheric plate, t is time and n an integer value.

Figure 6 shows *WLD*s data and the curve by Hoggard et al. (2017) of the plate model that best fits the global dataset, with d = 2380 m, H_o = 130 km and T_a = 1330 °C. To compare our *WLD*s estimated in the Herodotus and Levantine basins with those predicted by the plate-cooling model we need to fix the formation age. On this regard, two sources of data are available, namely Müller et al. (2008) and Granot (2016). From the analysis of marine magnetic anomaly data, the former claimed that the age of the Herodotus and Levantine basins ranges from 250-270 Ma, the latter estimated an age of the Herodotus crust of 340 ± 25 Ma. Therefore, it appears that depth data from the Levantine Basin do not fit the oceanic curve, as *WLD* is clearly lower than expected. Conversely, the Herodotus Basin data shows a good agreement with the predicted *WLD*. This again argues for the oceanic nature of the Herodotus Basin.

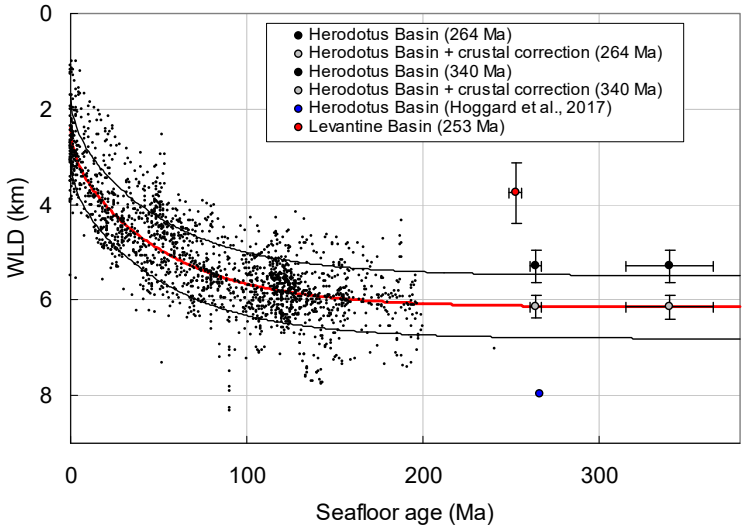

FIGURE 6. *WLD*s (black points) versus seafloor age from the global dataset and best-fitting plate cooling model (red curve) with ± one s.d. (black curve). Full circles: average *WLD* of the Levantine Basin (red) and in the Herodotus Basin only corrected for sediments (black) and after crustal correction (grey; see text). The blue circle is *WLD* in the Herodotus estimated by Hoggard et al. (2017).

If the Herodotus crust is of oceanic type, *WLD* data should be further corrected for the isostatic replacement of crustal thickness that differs from a reference crustal thickness with an equivalent water load (Hoggard et al., 2017). The crustal correction C_c is

$$C_c = \frac{\rho_a - \overline{\rho}_c}{(\rho_a - \rho_w)}(h_c - 7.1) \tag{9}$$

where h_c and $\overline{\rho}_c$ are the thickness and average density of oceanic crust, respectively, and 7.1 km is the global average crustal thickness after White et al. (1992) used to normalize the observed crustal thickness. By assuming an average crustal thickness in the Herodotus of 10 km (Crust 1.0 model) and assuming an oceanic crustal density of 2860 kg m^{-3} (Carlson and Herrick, 1990), C_c is about 850 m. This implies a further increase of the average estimated *WLD* of 6.2 ± 0.3 km, which thus fits better the oceanic curve (Fig. 6).

CONCLUDING REMARKS

The comparison between inferred water-load depth and the seafloor depth predicted by continental lithosphere stretching and ocean plate cooling models indicate that the Levantine Basin is likely to be a result for an old continental stretching event (> 250 Ma) whereas the Herodotus bathymetry is compatible with a 260-340 Ma old oceanic crust. This result of course strongly depends on the uncertainty on the *WLD* estimation, which in turn is mainly related to errors in bathymetric data and the thickness of the sediment cover. However, errors on our estimated *WLD*s do not appear critical.

Regarding the bathymetry, a comparison between the dataset used in this study (EMODnet) and other openly available seafloor files, namely ETOPO1 (Amante et al., 2009) and TOPEX (Smith and Sandwell, 1997) shows that the average differences in bathymetry are ~ 50 m. The sediment correction is instead more important. We carried out a preliminary analysis at two specific sites of the Herodotus and Levantine basin wherein detailed seismic information about the sediment thickness are available. In the Herodotus Basin, de Voogd et al. (1992) presented results of the expanding spread profile ESP18 (Fig. 2) indicating a thickness of the whole sediment cover in excess of about 1.4 km compared to the Crust 1.0 model. The seismic refraction and reflection records by Netzeband et al. (2006) along the profile P2 of the Levantine Basin (Fig. 2) shows that the sediment thickness of the Crust 1.0 model might be on average < 0.7 km. If we assume that the reference database assumed for this study underestimates the sediment thickness by ~ 1000 m, the uncertainty on the sediment correction, C_s, is of ~ 200 m.

In summary, the overall uncertainty due to sediment thickness and bathymetry errors is thus ~ 250 m. Error produced by uncertainties on the density assumed both for C_s and the crustal correction C_c are more difficult to quantify. By considering the typical average sediment thickness of the eastern Mediterranean, according to the error analysis suggested by (Hoggard et al., 2017), the error on Cs can be as large as ~ 200 m whereas it is negligible for Cc.

We found that *WLD*s in the Levantine Basin are significantly lower than values expected by the oceanic plate-cooling curve, thus supporting the continental nature of the lithosphere underlying the basin. In their analysis, Hoggard et al. (2017) estimated that *WLD* in the Herodotus Basin exceeds by about 2 km that predicted by the oceanic plate model (Fig. 6), thus suggesting a strong residual topography anomaly. We suggest that this anomaly is an artefact, caused by the inappropriate sediment correction applied by Hoggard et al. as in their global-scale study used values of solid grain density, ρ_{sg}, typical of oceanic sediments. In the Mediterranean Sea, the occurrence of thick evaporite layers within the sediment cover implies that density values of ocean sediments are not suitable. Pasquale et al. (2007), studied the *WLD* in the Southern Tyrrhenian and gave density values that can be adopted also for the Eastern Mediterranean, since sediment, types and depositional sequences are very similar. Therefore, we suggest that the *WLD* of the Herodotus Basin calculated in this paper are more likely and no residual topography anomaly is evident.

The eastern Mediterranean Sea seems characterized by a rather low terrestrial heat-flow. This is consistent with the low heat-flow values observed in the adjacent Ionian Sea (Pasquale et al., 2005). Although the average heat flow is similar in the Herodotus and Levantine basins, the latter exhibits a wider range (15-90 mW m^{-2}). The lowest values might be related to advective processes and therefore could not represent the regional thermal state. The highest heat-flow values could be instead produced by higher crustal radiogenic contribution, as they are located in an area of continental crustal thickening (Eratosthenes seamount). Since the two basins are likely to be older than ~ 250 Ma and they likely reached thermal equilibrium, the heat flow cannot be used to discriminate between oceanic and continental realms.

Further considerations on the thermal state of the eastern Mediterranean can be made through the analysis of the crustal radiogenic heat production. Figure 7, presents possible models of crustal composition of the Herodotus and Levantine basins as inferred from the seismic results. By assuming heat-production values as proposed by Inati et al. (2016) for the sediments, by Pasquale et al. (2005) for the oceanic crust and by Schütz et al. (2014) for the continental crust, the inferred crustal contribution to the surface heat flow in the Levantine Basin is twice that of the oceanic domain of the Herodotus Basin. This leads to a mantle heat flow of about 30 mW m^{-2}, which is nearly the same value of the mantle heat flow inferred in the Ionian lithosphere (Pasquale et al. 2005), whose oceanic nature is widely accepted (e.g. de Voogd et al. 1992). The mantle heat flow in the Levantine Basin is consistent with the range (27-24 ± 2 mW m^{-2}) inferred onshore by Schütz et al. (2014), southeast of the basin, in the Sinai continental microplate.

Despite the Levantine Basin has reached thermal equilibrium and therefore there is no evidence of extension in the surface heat flow, the crustal thickness still record lithosphere stretching that affected the area. From WLDs we estimated that stretching factor could vary from 1.6 to 2.7. Our estimate is consistent with factor β of 2.3-3.0 suggested by Netzeband et al. (2006) on the basis of seismic data.

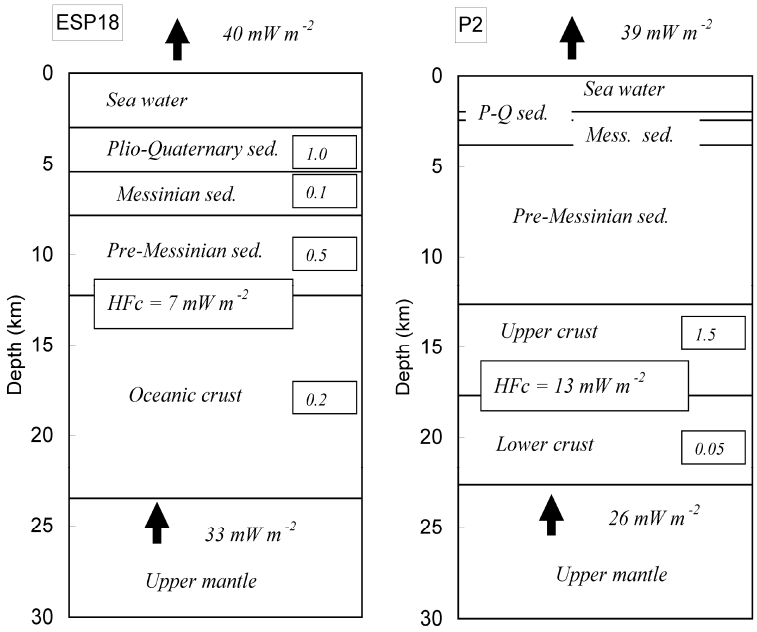

FIGURE 7. Crustal heat flow (HF) budget in the Herodotus (left) and Levantine (right) basins as inferred from seismic data of the expanding speard profile (ESP18) by de Voogd et al (1992) and seismic reflection/refraction data (P2) by Netzeband et al. (2006). The radiogenic heat production (in μW m^{-3}) of each layer is given.

REFERENCES

1. Aksu, A.E. Hall, J., Calon, T., Barnes, M.C., Güneş, P, Cranshaw, J.C., 2017. Messinian evaporites across the Anaximander Mountains, Sırrı Erinç Plateau and the Rhodes and Finike basins, eastern Mediterranean Sea. Marine Geology. 395, 48-64. doi: 10.1016/j.margeo.2017.09.013.
2. Amante, C., Eakins, B.W., 2009. ETOPO1 1 Arc-Minute Global Relief Model: Procedures, Data Sources and Analysis. NOAA Technical Memorandum NESDIS NGDC-24, 19 pp.
3. Athy, L.F., 1930. Density, Porosity and Compaction of Sedimentary Rocks. Bulletin of the American Association of Petroleum Geologists (AAPG Bulletin), 14, 1-24.
4. Ben Avraham, Z., Ginzburg, A., Makris, J., Eppelbaum, L., 2002. Crustal structure of the Levant Basin, Eastern Mediterranean. Tectonophysics, 346 (1–2), 23–43. doi: 10.1016/S0040-1951(01)00226-8.
5. Carlson, R., Herrick, C.N., 1990. Densities and porosities in the oceanic crust and their variations with depth and age. Journal of Geophysical Research Atmospheres, 95(B6), 9153-9170. doi: 10.1029/JB095iB06p09153.
6. Chiozzi P., Verdoya M., 2018. Heat-flow anomaly and residual topography in the Mascarene hotspot swell (Indian Ocean) Int J Earth Sci (Geol Rundsch) 107: 35–51.
7. Christensen, U., 1982. Phase boundaries in finite amplitude mantle convection. Geophysical Journal of the Royal Astronomical Society. Volume 68, Issue 2. doi: 10.1111/j.1365-246X.1982.tb04911.x
8. Conrad, C.P., Husson, L., 2009. Influence of dynamic topography on sea level and its rate of change. Lithosphere, v.1, no. 2, 110-120. doi: 10.1130/L32.1
9. Cowie, L., Kusznir, N., 2012. Gravity inversion mapping of crustal thickness and lithosphere thinning for the eastern Mediterranean. The Leading Edge, 31(7), 810-814. doi: 10.1190/tle31070810.1
10. Crosby, A.G., McKenzie, D., Sclater, J.G., 2006. The relationship between depth, age and gravity in the oceans. Geophys J Int 166, 553-573. doi: 10.1111/j.1365-246X.2006.03015.x.
11. Crosby, A.G., McKenzie, D., 2009. An analysis of young ocean depth, gravity and global residual topography. Geophys J Int 178, 1198-1219. doi: 10.1111/j.1365-246X.2009.04224.x.
12. Dercourt, J., Zonenshain, L.P., Ricou, L.E., Kazmin, V.G., Le Pichon, X., Knipper, A.L., Grandjacquet, C., Sbortshikov, I.M., Geyssant, J., Lepvrier, C., Pechersky, D., Boulin, J., Sibuet, J.C., Savostin, L.A., Sorokhtin, O., Westphal, M., Bazhenov, M., Lauer, J.P., Biju-Duval, B., 1986. Geological evolution of the Tethys belt from the Atlantic to the Pamirs since the LIAS. Tectonophysics. 123. 241-315. 10.1016/0040-1951(86)90199-X.
13. Domeier, M., Torsvik, T. H., 2014. Plate tectonics in the late Paleozoic. Geoscience Frontiers Volume 5, Issue 3, 303_350.
14. de Voogd, B. Truffert C., Chamot-Rooke N.,. Huchon P,. Lallemant S., Le Pichon X, 1992. Two-ship deep seismic soundings in the basins of the Eastern Mediterranean Sea (Pasiphae cruise) *Geophys. J. Int.* 109, *536-5.52*
15. Erickson, A. J., 1970. The Measurements and Interpretation of Heat flow in the Mediterranean and Black Sea, Ph.D. Thesis (M.I.T., Cambridge, Massachusetts,).
16. Erickson, A.J., Simmons, G., Ryan, W.B.F., 1977. Review of Heat Flow Data from the Mediterranean and Aegean Seas. In International Symposium of the Structural History of the Mediterranean Basins (eds. BIJU-DUVAL, B. and MONTADERT, L.) (Editions Technip) pp. 263–280.
17. Erickson, A.J., Von Herzen, R.P., 1978. Down-hole Temperature Measurements, Deep Sea Drilling Project. Leg 42A. In Initial Reports of the Deep Sea Drilling Project, 42, Part I (eds. HSU, K.J., MONTADERT, L. et al.) (Washington U.S. Government Printing Office) pp. 857–871.
18. Gardosh, M., Druckman, Y., Buchbinder, B., Rybakov, M., 2006. The Levant Basin offshore Israel: stratigraphy, structure, tectonic evolution and implications for hydrocarbon exploration. Geophysical Survey of Israel, p.1–119.
19. Garfunkel, Z., 1998.Constraints on the origin and history of the Eastern Mediterranean basin. Tectonophysics 298, 5-35.
20. Gennesseaux M., Burollet P. Winnock E., 1998. Thickness of the Plio-Quaternary sediments (IBCM-PQ) Bollettino di Geofisica Teorica Ed Applicata VOL. 39, N. 4, pp. 243-284.
21. Granot, R., 2016. Palaeozoic oceanic crust preserved beneath the eastern Mediterranean. Nat. Geosci. 9 (9), 701–705. http://dx.doi.org/10.1038/ngeo2784.
22. Hall, J.K., Calon, T.J., Aksu A.E., Meade, S.R., 2005. Structural evolution of the Latakia Ridge and Cyprus Basin at the front of the Cyprus Arc, Eastern Mediterranean Sea. Mar Geol, 221, 261–297. doi: 10.1016/j.margeo.2008.02.007
23. Heine, C., Müller, D., 2008. The IntraCONtinental basins (ICONS) atlas – Applications in eastern Australia. 275-290.
24. Hoggard, M.J., Winterbourne, J., Czarnota, K., White, N., 2017. Oceanic residual depth measurements, the plate cooling model, and global dynamic topography. Journal of Geophysical Research: Solid Earth/Volume 122, Issue 3. 2328- 2373. doi: 10.1002/2016JB013457
25. Inati, L., Zeyen, H., Nader, F.H., Adelinet, M., Sursock, A., Rahhal. M.E., Roure, F., 2016. Lithospheric architecture of the Levant Basin (Eastern Mediterranean region): A 2D modeling approach. Tectonophysics, 693, 143-156.

26. Işler, F.I., Aksu, A.E., Hall, J., Calon, T., Yasar, D., 2005. Neogene development of the Antalya Basin, Eastern Mediterranean: An active forearc basin adjacent to an arc junction. Marine Geology. 221. 299-330. doi: 10.1016/j.margeo.2005.03.006.
27. Laske, G., Masters, G., Ma, Z., Pasyanos, M., 2013. Update on CRUST1.0 - A 1-degree global model of Earth's crust. Abstract EGU2013-2658 presented at 2013 Geophys. Res. Abstracts 15. 15. 2658-.
28. Le Pichon, X., Sibuet, J.C., 1981. Passive margins: a model of formation. J. Geophys. Res. 86, 3708–3720.
29. Majorowicz, J., Wybraniec, S., 2011. New terrestrial heat-flow map of Europe after regional paleoclimatic correction application, *Int. J. Earth Sci.,* 100, 881–887.
30. McKenzie, D., 1978. Some remarks on the development of the sedimentary basins. Earth Planet. Sci. Lett. 40: 25-32.
31. Morgan, P. (1973), Terrestrial Heat Flow Studies in Cyprus and Kenya, Ph.D. Thesis, University of London.
32. Morgan P., 1979. Cyprus hat flow with comments on the thermal regime of the eastern Mediterranean. In Terrestrial Heat Flow in Europe eds V. Cermak et al. Springer-Verlag Berlin Heidelberg pp144-151.
33. Müller, R.D., Sdrolias, M., Gaina, C., Roest, W., 2008. Age, spreading rates, and spreading asymmetry of the world's ocean crust. Geochem Geophys Geosys 9, Q04006. doi:10.1029/2007GC001743
34. Netzeband, G.L., Gohl, K., Hübscher C.P., Ben-Avraham Z., Dehghani G.A., Gajewski D., Liersch, P., 2006. The Levantine Basin - crustal structure and origin: Tectonophysics, 418, 167-188.
35. Parsons, B., Sclater, J.G., 1977. An analysis of the variation of ocean floor bathymetry and heat flow with age. J Geophys Res, 82, 803-827.
36. Pasquale, V., Verdoya, M., Chiozzi, P., 1994. Types of crust beneath the Ligurian Sea. Terra Nova, 6, 255–266.
37. Pasquale, V., Verdoya, M., Chiozzi, P., 1995. Rifting and thermal evolution of the Northwestern Mediterranean. Ann. Geofis., 38, 43–53.
38. Pasquale V., Verdoya M., Chiozzi P., 2005. Thermal Structure of the Ionian Slab Pure appl. geophys. 162 967–986
39. Pasquale V., Chiozzi P., Verdoya M. 2007. Isostasy and paleotemperatures in the Southern Tyrrhenian Basin, Mediterranean Sea Mar Geophys Res (2007) 28:139–151.
40. Pribnow, D.F.C., Kinoshita, M., Stein, C.A., 2000. Thermal Data Collection and Heat Flow Recalculations for ODP Legs 101-180, Institute for Joint Geoscientific Research, GGA, Hannover, Germany, 0120432.
41. Roberstson, A.H.F., 1998. Tectonic significance of the Eratosthenes Seamount: a continental fragment in the process of collision with subduction zone in the eastern Mediterranean (Ocean Drilling Program Leg 160). Tectonophysics, 298, 63–82.
42. Salamon, A., Hofstetter, A., Garfunkel, Z. and Ron, H., 1996. Seismicity of the eastern Mediterranean region: Perspective from the Sinai subplate. Tectonophysics 263: 293-305.
43. Sandwell, D.T., Müller, R.D., Smith, W.H.F., Garcia, E., Francis, R., 2014. New global marine gravity model from CryoSat-2 and Jason-1 reveals buried tectonic structure. Science 346(6205):65–67. doi:10.1126/science.1258213
44. Sawyer, D., 1985. Total tectonic subsidence: A parameter for distinguishing crust type at the U. S. Atlantic Continental Margin. Journal of Geophysical Research. 90. 7751-7770. doi: 10.1029/JB090iB09p07751.
45. Schütz, F., Förster, H.J., Förster, A., 2014. Thermal conditions of the central Sinai Microplate inferred from newsurface heat-flow values and continuous borehole temperaturelogging in central and southern Israel Journal of Geodynamics 76 8–24
46. Smith, W.H.F., Sandwell, D.T, 1997. Global sea floor topography from satellite altimetry and ship depth soundings. Science, 277, 1956-1962
47. Stampfli, G., Marcoux, J. Baud, A., 1991.Tethyan margins in space and time. Palaeogeogr. Palaeoclimatol. Palaeoecol. 87, 373_409
48. Stein, C.A. Stein, S., 1992. A model for the global variation in oceanic depth and heat flow with lithospheric age. Nature, 359, 123-129. doi:10.1038/359123a0
49. Turcotte, D. L., and G. Schubert, 2002. *Geodynamics*, 2nd ed., Cambridge Univ. Press, Cambridge, U. K.
50. Von Herzen, R., Uyeda, S., 1963. Heat flow through the eastern Pacific Ocean floor. J Geophys Res 68:4219–4250
51. Welford, K., Hall, J., Rahimi, A., Reiche, S., Huebscher, C., Louden, K., 2015. Crustal structure from the Hecataeus Rise to the Levantine Basin, eastern Mediterranean, from seismic refraction and gravity modelling. Geophysical Journal International. 203. 2055-2069. doi: 10.1093/gji/ggv422.
52. White, R.S., McKenzie, D., O'Nions, R. K., 1992, Oceanic crustal thickness from seismic measurements and rare earth element inversions: Journal of Geophysical Research, v. 97, p. 19683–19715.